International Journal of Engineering Research & Technology (IJERT)
ISSN: 2278-0181
Vol. 8 Issue 06, June-2019

Synthesis and Morphological Characterization of Nickel-Zinc Oxide Composites using Solid State Method

Sani Garba Danjumma
Department of Sciences
Kebbi State Polytechnic, Dakingari,
Nigeria

Abubakar Yakubu
Department of Physics
Kebbi State University of Science and Technology,
Aliero, Nigeria

Sirajo Abdullahi
Department of Physics
Kebbi State University of Science and Technology,
Aliero, Nigeria

Saidu Aliyu
Department of Sciences
Kebbi State Polytechnic, Dakingari,
Nigeria

***Abstract*- Some properties of materials are functions of their microstructures, and, consequently, of their thermal histories. It is often the case that these properties are more desirable than those associated with the equilibrium state. Many times, the physical properties and, in particular, the mechanical behaviour of a material depend on the microstructure. Microstructure is subject to direct microscopic observation, using optical or electron microscopes. The synthesis of a doped zinc-oxide composites using simple solid stated method was successfully carried out in this research. Characterization were carried out for the surface morphology and bonding of the composites using SEM and FTIR, respectively. The result from SEM was able to distinguish between the filler and matrix for each composition. The result also revealed agglomeration of particles as doping increased for all compositions. As doping increased to higher quantity, density of sample increased and this allowed for the faster propagation of light through the sample, which is evident in the FTIR analysis. All results obtained were promising for microwave absorption applications.**

Key Words: Synthesis, Morphological, Characterization, Nickel-Zinc Oxide, Composites

I. INTRODUCTION

Composites are artificially produced multiphase materials having a desirable combination of the best properties of the constituent phases. With knowledge of the various types of composites, as well as an understanding of the dependence of their behaviours on the characteristics, relative amounts, geometry/distribution, and properties of the constituent phases, it is possible to design materials with property combinations that are better than those found in the metal alloys, ceramics, and polymeric materials. ZnO is a wide band gap (3.2 eV) n-type semiconductor that has found a wide range of applications as a transparent conducting oxide (TCO) electrode in photovoltaics, photocatalysis, sensing, fuel cells and other optoelectronic devices (Albert & Abiola, 2017). Umit, (2010), reported that, ZnO is an attractive material for applications in electronics, photonics, acoustics, and sensing. In optical emitters, its high exciton binding energy (60 meV) gives ZnO an edge over other semiconductors such as GaN if reproducible and reliable p-type doping in ZnO were to be achieved, which currently remains to be the main obstacle for realization of bipolar devices. On the electronic side, ZnO holds some potential in transparent thin film transistors (TFTs) owing to its high optical transmittivity and high conductivity.

NiO is a p-type wide band gap (4.2 eV) semiconductor that has been used in similar applications. ZnO and NiO readily form a p-n junction that has shown good electrical properties for gas sensing, fuel cell electrodes and photocatalysis (Albert and Abiola, 2017). The applications of Nickel oxide (NiO) today is found in semiconductors, capacitor–inductor devices, tuned circuits, transparent heat mirrors, thermistors and varistors, batteries, micro-supercapacitors, electrochromic and chemical or temperature sensing devices. It is used in preparation of nickel cermet, plastics and textiles, in nanowires, nanofibers and specific alloy and catalyst applications. It is also used as an antiferromagnetic layers, accelerators and radar absorbing materials, aerospace and active optical filters (Sani *et al*., 2019; AzoNano, 2013). Sónia *et al*. (2017), focuses on the production by powder metallurgy of aluminum and nickel matrix composites reinforced by CNTs, using ultrasonication as the dispersion and mixture process. Microstructural characterization of nanocomposites was performed by scanning and transmission electron microscopy (SEM and TEM) and the result revealed that, CNT clusters at grain boundary junctions were also observed. Abdul *et al.* (2017), in their work describes the fabrication of Ni–graphene composite coatings on carbon steel at different deposition temperatures (15^0C, 30^0C, 45^0C and 60^0C, respectively) by an electrochemical co-deposition method. The surface morphology was examined by scanning electron microscopy (SEM), and the results showed that the Ni–graphene composite coatings deposited at 45^0C exhibit coarser surface morphology with increased carbon content.

Nickel/cobalt double hydroxides with sphere-like nanoflowers and nanoporous structures were controllably prepared by introducing halide ions into the reaction system. The morphology and structure of the composites were characterized by X-ray diffraction, scanning electron microscope, infrared spectra and Brunauer-Emmett-Teller method. Halides, especially bromide, can dramatically affect the morphology of the crystal aggregates, and some

International Journal of Engineering Research & Technology (IJERT)
ISSN: 2278-0181
Vol. 8 Issue 06, June-2019

morphology-dependent electrochemical properties are found (Yuqing, 2018).

Dispersion of 2D carbon nitride (C_3N_4) nanosheets into a nickel phosphorous (NiP) matrix was successfully achieved by ultrasonication during the electroless plating of NiP from an acidic bath. The morphology and thickness were determined by scanning electron microscopy and energy-dispersive X-ray spectroscopy. C_3N_4 showed a homogeneous distribution morphology in the nanocomposite that changed from amorphous in case of the NiP to a mixed crystalline-amorphous structure in the NiP-C_3N_4 nanocomposite (Eman *et al.*, 2018).

Synthesized NiO are used to prepare Polyaniline (PANI)-NiO nanocomposites by in situ chemical oxidative polymerization at 0-50C. Different weight percentages of NiO were added during the polymerization. PureNiO, shows small spherical shaped Pure NiO. PN-5 shows the encapsulation of NiO nano particles by polyaniline with flower like structure. PN-20 and PN-40 depicts spherical shaped structures with cluster formation. FTIR shows weak Van der Waals forces of attraction between metal oxide and polymerised aniline (Rajashekhar *et al*., 2015). Kazuaki *et al.*, (2011), reported that, the SEM of NZF/PEG (Ni-Zn ferrite/pentaerythritol tetra-polyethylene glycol ether) and NZF/ER composites, revealed voids between particles are observed. On the other hand, they are not found in the NZFN/PEG composite; therefore, NZFN/PEG composites can be formed a densely-packed microstructure.

The FTIR spectra for pure PVA, ZnO/ PVA nanocomposite films and ZnO are reported by Mansour, *et al*. (2014). In the spectra of pure PVA and ZnO/ PVA nanocomposites, the broad and strong band centered at 3340 cm−1 is assigned to the stretching vibration of hydroxyl group (OH). The strong band at 2940 cm−1 is assigned to the band of asymmetric CH_2 stretching. The two bands observed at 1712 and 1658 cm−1 are assigned to the stretching vibrational band of C=O. The two bands observed at 1427 and 1330 cm-1 are assigned as CH_3 bending vibration and CH2 stretching respectively. The band at 1090 cm^{-1} arises from the C–O stretching vibration while the band at 920 cm-1 results from CH_2 rocking vibration. Also, the band at 850 cm^{-1} result from C–C stretching vibration and that at 660 cm^{-1} arises from out of plane OH bending. The band at 432cm^{-1} is assigned to the stretching vibration of Zn-O bond. FTIR spectra of PVA, ZnO and ZnO/ PVA nanocomposites indicating that there are no interactions between polyvinyl alcohol and zinc oxide in forming nanocomposites.

The effect of SiO_2 addition on the properties of ZnO-NiO composite were investigated by Osama *et al*. (2014). They reported that, the SEM of their sample, shows the segregation of the intergranular phase in patches. This is evident from the different shades displayed varying from dark grey – light grey and white. The samples were of very dense microstructure. Although some pores were present, they were very small and separated from one another. The decrease of grain size is attributed to the precipitation of secondary phase in the grain boundaries and nodal points. The ZnO grains are homogeneous, NiO SiO_2 particles are small and distributed at the boundary of the ZnO grains.

Shanavas *et al*., (2019), repoted the surface images of PANI, ZnO nanoparticles, and PANI/ZnO nanocomposite. The SEM image of PANI; has various structures such as granules, nanofibers, nanotubes, nanospheres, and microsphere. The diameter of PANI is approximately 100nm, and they have an irregular road-like morphology. The morphology of PANI has changed by the introduction of ZnO nanoparticles, it can be concluded that a thin layer of PANI molecules was adsorbed on the surface of ZnO nanoparticles, and a core-shell structure of ZnO/PANI nanocomposite with the core of ZnO inorganic nanoparticle and the shell of monolayer PANI chains has been formed. The ZnO nanoparticles have a crystalline spherical structure. They went further to report that, the FTIR spectrum of ZnO nanoparticles in which the characteristic peaks at 430 cm^{-1} and 496 cm^{-1} is related to the Zn-O stretching mode. According to the patterns, absorption intensity is increased by adding ZnO nanoparticles in the case of nanocomposites due to the uniform distribution of ZnO nanoparticles in nanocomposite matrix and elimination of agglomeration.

Jacek *et al.* (2018), present selected representative SEM images of $Zn_{0.9}Co_{0.1}O$ NPs samples. An impact of the change of H_2O content in the precursor on the morphology and size of $Zn_{0.9}Co_{0.1}O$ NPs was observed. Powders obtained from the precursor with the water contents of 1.5% and 2% are composed of compact structures resembling a “cauliflower” structure. NPs obtained from the precursor with the H_2O content of 3, 4, and 5% had a homogeneous and loose structure.

Various layers with different ZnO nanopowder/grapheme nanoplatelets content, the respective ratio varying between 0.33 and 1.5, were prepared and studied by Drakakis *et al.* (2018). They present SEM images of the commercial graphene nanoplatelets, the composite with the lowest ZnO nanopowder concentration and the composite with the highest ZnO nanopowder concentration. The images indicate that all the materials are very conductive (they are quite transparent for the electron beam) and the graphene flakes are quite flat even in the composite. Composite materials are homogeneous and ZnO has a more or less uniform distribution in the composites bulk as small agglomerations, which are more pronounced in the case of the highest ZnO nanopowder concentration. Moreover, the graphene flakes keep their general aspect in the composite materials (they don't agglomerate or crinkle very much), being decorated with ZnO nanoparticles agglomerations.

Most of the researches reported did not explore the suitability of their composites in microwave absorption. For this reason, the suitability of the prepared composites is characterized to study its suitability in microwave absorption.

II. SAMPLE PREPARATION

In our work, the solid state method is used in the preparation of a doped zinc oxide. The materials used for the synthesis are 100 g of Zinc oxide (99.7% purity) and 50 g of Nickel oxide (99.7% purity) all in powdered form. The Zinc oxide was obtained at Halishuaib Chemicals while the Nickel oxide was obtained at CEMAN Chemicals Ventures. During the preparation of the composites, 5 g of Nickel oxide was

International Journal of Engineering Research & Technology (IJERT)
ISSN: 2278-0181
Vol. 8 Issue 06, June-2019

mixed with 25 g of Zinc oxide using pestle and mortar, the combination was grinded continuously using mortar and pestle for about 60 minutes for perfect homogeneity. The mixed sample was taken to furnace and was heated to about 1000^0C for appreciable reaction to take place. The same procedure was applied for 7.5 g of Nickel oxide and 22.5 g of Zinc oxide, 10 g of Nickel oxide and 20 g of Zinc oxide, 12.5 g of Nickel oxide and 17.5 g of Zinc oxide, and 15 g of Nickel oxide and 15 g of Zinc oxide.

Five different mixtures with different proportions of Zinc oxide and Nickel oxide were prepared. The summary of materials composition is shown in Table 1. The prepared composites are then ready for characterization.

TABLE 1: COMPOSITION OF SAMPLES

Sample	NiO		ZnO		Total	
	(g)	*%*	*(g)*	*%*	*(g)*	*%*
A	5.0	16.7	25.0	83.3	30.0	100
B	7.5	25.0	22.5	75.0	30.0	100
C	10.0	33.3	20.0	66.7	30.0	100
D	12.5	41.7	17.5	58.3	30.0	100
E	15.0	50	15.0	50	30.0	100

III. CHARACTERIZATION

Characterization of the samples were carried out using FTIR-8400S for chemical bonding and absorption pattern of the samples while SEM machine Inspect S50 microscope was used to study the surface morphology of matrix and filler.

IV. RESULTS AND DISCUSSION

A. FTIR

Fig. 1 to 3 are the results obtained from FTIR spectroscopy for the 16.7 %, 25.0 % and 33.3 % doped ZnO composites, respectively. They were acquired in the range of 750 to 4000 cm^{-1} wavenumber, with a maximum transmittance of 100 %.

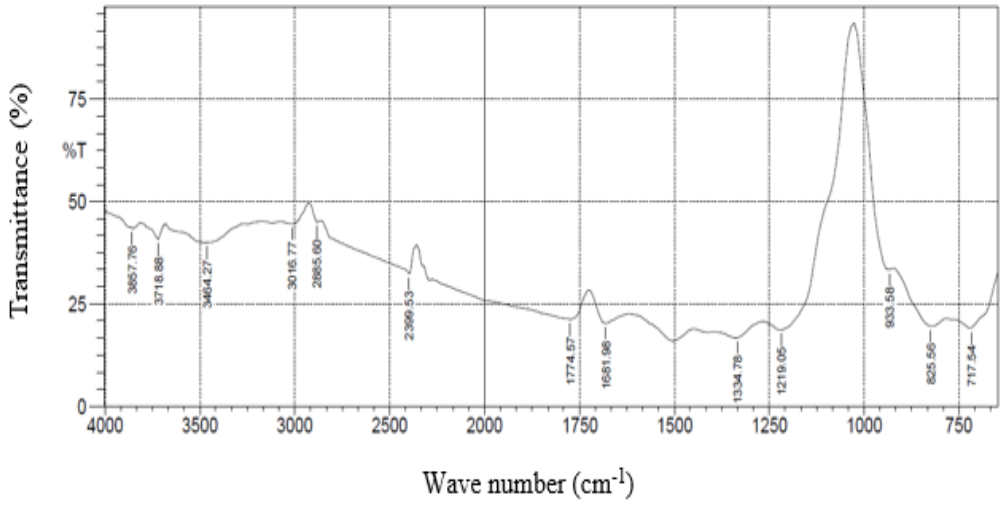

Fig. 1: FTIR Spectra for 16.7 % Doped ZnO

Observation on Fig. 1, shows the absorption region of 717.54 cm^{-1}, 825.50 cm^{-1}, 1219.05 cm^{-1}, 1334.78 cm^{-1}, 1681.98 cm^{-1} and 1774.57 cm^{-1}. The highest absorbance observed is 83.3 % at 1334.78 cm^{-1} peak corresponding to 16.7 % of transmittance. The absorption band observed at 717.54 cm^{-1} corresponds to C-Cl stretching vibrations and the one at 825.50 cm^{-1} attributes C-C skeletal vibrations. The band at 1219.05 cm^{-1} corresponds to C-N stretching vibrations. The band appearing at 1334.78 cm^{-1} attributed to C-H bending vibration. The band at 1681.98 cm^{-1} corresponds to the symmetrical of C=O. The band at 1774.57 cm^{-1} attributes the C=O stretching (Assem *et al.*, 2013).

International Journal of Engineering Research & Technology (IJERT)
ISSN: 2278-0181
Vol. 8 Issue 06, June-2019

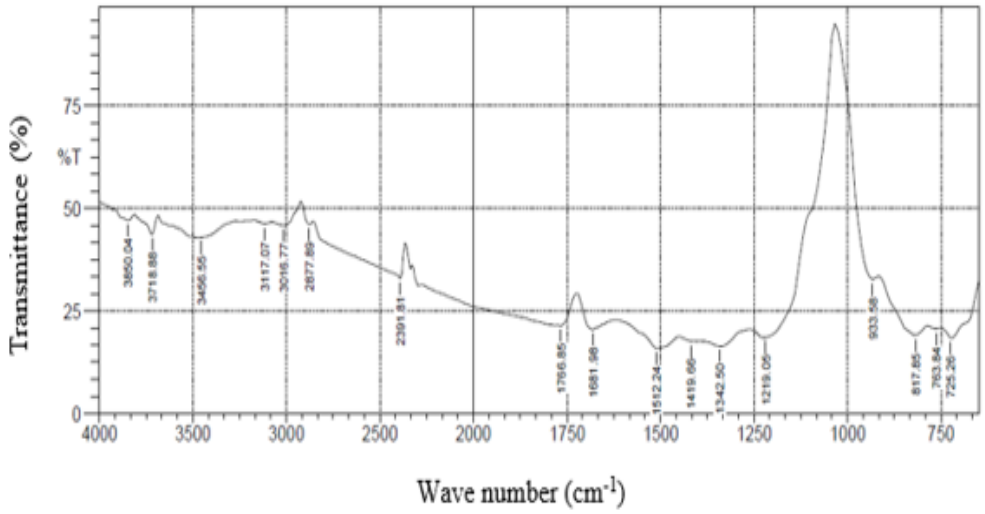

Fig. 2: FTIR spectra for 25.0 % Doped ZnO

Fig. 2 shows the absorption region of 725.26 cm^{-1}, 763.84 cm^{-1}, 817.85 cm^{-1}, 1219.05 cm^{-1}, 1342.50 cm^{-1}, 1419.00 cm^{-1}, 1512.24 cm^{-1}, 1681.98 cm^{-1} and 1766.85 cm^{-1}. The highest absorbance recorded is around 84.1 % at 1512.24 cm^{-1} corresponding to 15.9 % of transmittance. The absorption band observed at 725.26 cm^{-1} and 763.84 cm^{-1}corresponds to strong C-Cl stretching. The band at 817.85 cm^{-1} attributes C-C skeletal vibrations. The absorption at 1219.05 cm^{-1} corresponds to C-N stretching vibrations. The band appearing at 1342.50 cm^{-1} attributed to C-H bending vibration. The band at 1419.00 cm^{-1} corresponds to asymmetric C-H bending. The absorption band at 1512.24 cm^{-1} attributes to C-H skeletal vibrations. The band at 1681.98 cm^{-1} corresponds to the symmetrical of C=O. The band at 1766.84 cm^{-1} attributes the C=O stretching (Yakubu *et al.*, 2017).

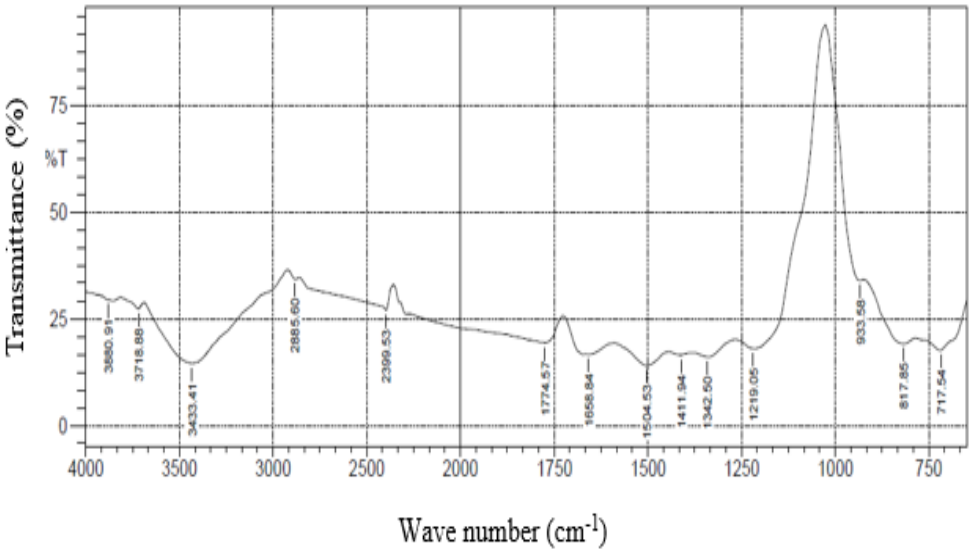

Fig. 3: FTIR Spectra for 33.3 % Doped ZnO

Careful observation on Fig. 3 shows the absorption the region of 717.54 cm^{-1}, 817.85 cm^{-1}, 1219.05 cm^{-1}, 1342.50 cm^{-1}, 1411.94 cm^{-1}, 1504.53 cm^{-1}, 1658.84 cm^{-1}, 1774.57 cm^{-1} and 3433.41 cm^{-1}. The highest absorbance observed is 86 % at 1504.53 cm^{-1} corresponding to 14% transmittance. The absorption band observed at 717.54 cm^{-1} corresponds to strong C-Cl stretching and the one at 817.85 cm^{-1} attributes C-C skeletal vibrations. The absorption at 1219.05 cm^{-1} corresponds to C-N stretching vibrations. The band appearing at 1342.50 cm^{-1} attributed to C-H bending vibration. The band at 1411.94 cm^{-1} corresponds to asymmetric C-H bending. The band at 1658.84 cm^{-1} corresponds to the symmetrical of C=O. The band at 1774.57 cm^{-1} attributes the C=O stretching and the one at 3433.41 cm^{-1} corresponds to strong O-H stretching (Yakubu *et al.*, 2015a).

The 33.3 % doped composites showed the highest absorption which indicates increase in absorption as doping quantity increases. Depicted in Table 2 is the summary of the quantity of absorption as evident in the FTIR analysis for all samples prepared.

International Journal of Engineering Research & Technology (IJERT)
ISSN: 2278-0181
Vol. 8 Issue 06, June-2019

TABLE 2: SUMMARY OF ABSORPTION FOR ALL SAMPLES

S/N	Doped ZnO (%)	Absorption (%)
1	16.7	83.3
2	25.0	84.1
3	33.3	86.0

B. SEM

Careful observation on Fig. 6(a), shows defined coarse morphology with uniform particles that are agglomerated and forms irregular shaped particles. The darks spots indicates NiO with less density in distribution while the white spots indicates ZnO (Ahmad *et al*., 2015). Further observation shows a denser coarse morphology attributed to the increase in the filler content. From Fig. 6(b), the micrograph shows some whitish color image indicating the presence of zinc oxide, which are agglomerated by some doted NiO. Fig. 6(c) shows a micrographs with whitish colour image agglomerated with dark dotes of NiO (Karthikeyan *et al*., 2017). Due to the density of the sample in Fig. 6(d), more light were able to pass through it which is evident in the FTIR analysis. Observation on Fig. 6(e) shows that the zinc oxide and filler are sparsely dispersed through the matrix of the composite materials, and visible traces of white and black coloring are seen indicating the equal percentage of mixture in the sample (Yakubu *et al*., 2015b).

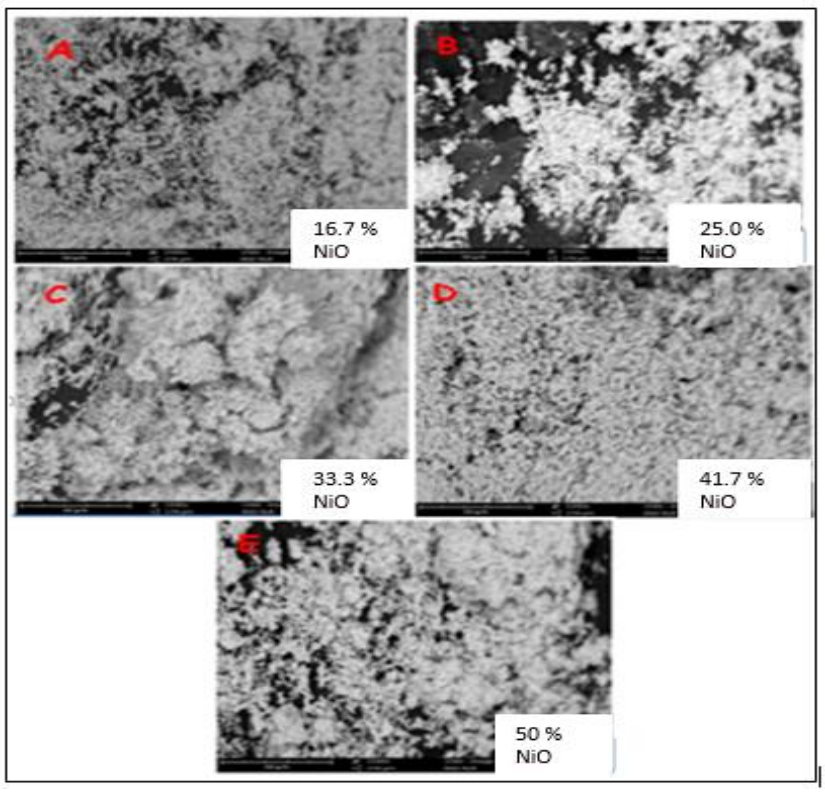

Fig. 6: SEM micrographs for doped composites

V. CONCLUSION

The synthesis of a doped zinc-oxide composites using simple solid stated method was successfully carried out in this research. Based on the investigations carried, result from SEM was able to distinguish between the filler and matrix for each composition. In addition the result also revealed agglomeration of particles as doping increased for all compositions. As doping increased to higher quantity, density of sample increased and this allowed for the propagation of light through the sample, which is evident in the FTIR analysis. It is then concluded that the samples prepared can be suitable for microwave absorption.

REFERENCES

[1] Abdul, J., Ghulam, Y., Waheed, Q. K., Yousaf, A. M., Rashid, M. K., Muhammad, N. N., & Ghulam, M. (2017). Electrochemical deposition of nickel grapheme composite coatings: effect of deposition temperature on its surface morphology and corrosion resistance. *Royal Society of Chemistry*, Vol.7, pp.311.

[2] Ahmad, F., Zulkifly, A., Mohamad, F. Z., Suzan, J., & Yakubu, A. (2015). Dielectric characterization of oil palm fiber reinforced polycaprolactone-nickel oxide composite at microwave frequency. *Procedia Environmental Sciences*, *30*, 273 – 278.

[3] Ajai, K. S. M., & Sangshetty, K. (2017). Preparation, Structural and Dielectric Properties of Polyaniline-Nickel Ferrite Composites. *International Journal of Materials Science*, 12, 47-56.

[4] Albert, O. J., & Abiola, M. (2017). Synthesis and structural analysis of ZnO-NiO mixed oxide nanocomposite prepared by homogeneous precipitation. *Ceramics International*, *43*(2017), 15424–15430.

[5] Assem, B., Mousa, A., Mohammed, S., Abdullah, S. A., Belkheir, H., Taibi, B. H., Salim, F. H., Ahmed, B., & Ismail, W. (2013). One Step Synthesis of NiO Nanoparticles via Solid-State Thermal Decomposition at Low-Temperature of Novel *Aqua* (2,9-dimethyl-1,10-phenanthroline)$NiCl_2$ Complex. *Int. J. Mol. Sci.*, 14, 23941-23954.

[6] AzoNano, (2013), Nickel Oxide (NiO) Nanoparticles: Properties, Applications. Retrieved from www.azonano.com/article.aspx?ArticleID=3378 on 7th February, 2019.

[7] Drakakis, E., Suchea, M., Tudose, V., Kenanakis, G., Stratakis, D., Dangakis, K., Miaoudakis, A., Vernardou, D., & Koudoumas, E. (2018). Zinc oxide-graphene based composite layers for electromagnetic interference shielding in the GHz frequency range. *Thin Solid Films*, v651, 152–157.

[8] Eman, M. F., Aboubakr, M. A., Mohammad, K. H., Adel, M. M., Chuhong, W., George, J., & Zoheir, F. (2018). Synthesis, Characterization, and Application of Novel Ni-P-Carbon Nitride Nanocomposites. *Coatings 2018*, 8, 37.

[9] Jacek, k., Tadeusz, C., Stanisław, G., Kamil, S., & Witold, L. (2018). Size Control of Cobalt-Doped ZnO Nanoparticles Obtained in Microwave Solvothermal Synthesis. *Crystals*, 8(179), 1-18.

[10] Karthikeyan, V., Padmanaban, A., Dhanasekaran, T., Praveen Kumar, S., & Gnanamoorthy, G. (2017). Synthesis and Characterization of ZnO/NiO and Its Photocatalytic Activity. *Mechanics, Materials Science & Engineering Journal*, 9.

[11] Kazuaki, S., Kiyotaka, F., Nobuyuki, M., Nobuki, T., & Satoshi, S. (2011). Microwave Absorption Properties of Polymer Modified Ni-Zn Ferrite Nanoparticles. *Materials Transactions*, 52(4), 740-745.

[12] Mansour, A.F., Mansour, S.F. and Abdo M. A., (2015. Improvement Structural and Optical Properties of ZnO/ PVA Nanocomposites. *IOSR Journal of Applied Physics (IOSR-JAP), 7*, 60.

[13] Osama, A. D., Mostafa, M. H., Khalil, K., & Hamdy, A. K. (2015). Microstructure and Dielectric Properties of ZnO-SiO2-NiO Composite. *International Journal of Science and Research (IJSR)*, 316-323.

[14] Rajashekhar, B., Vishnuvardhan, T. K., Shashidhar, N., Satishkumar, K. B., Basavaraja, C., & Chandrashekhar, M. (2015). Synthesis, Characterization and Study of Electrical Properties of Polyaniline-NiO Nanocomposites. *International Journal of Research in Engineering and Applied Sciences*. 5(7), 36-46.

[15] Sani, G. D., Yakubu, A., & Sahabi, S. (2019). Nickel Oxide (NiO) Devices and Applications: A Review. *International Journal of Engineering Research & Technology (IJERT)*, 8(04), 461-467.

[16] Shanavas, J., K., Asha, R., & Beena, B., (2018). Polyaniline/Zinc Oxide Nanocomposite as a Remarkable Antimicrobial Agent in Contrast with PANI and ZnO. *Indian Journal of Advances in Chemical Science*, 71.

[17] Sónia, S., Filomena, V., Marcos, A. L. R., & Manuel F. V. (2017). Aluminum and Nickel Matrix Composites Reinforced by CNTs: Dispersion/Mixture by Ultrasonication. *Metals 2017*, *7*, 1.

[18] Umit, O. (2010). ZnO Devices and Applications: A Review of Current Status and Future Prospects. *Proceedings of the IEEE*, *98*(7), 1255-1268.

[19] Yakubu, A., Abbas, Z., Esa, F., & Tohidi P., (2017). The effect of ZnO Nanoparticle filler on the attenuation of ZnO/PCL Nanocomposites using microstrip line at microwave frequency. *International polymer processing*, Volume 30. Retrieved on 15/01/17 from www.hanser-elibrary.com/doi/abs/10.3139/217.015022.

[20] Yakubu, A., Zulkifly, A., Mansor, H., & Ahmad, F. (2015a). Effect of Sintering Temperature on $Co_{0.5}Zn_{0.5}Fe_2O_4$ Nano-Particles Evolution and Particle Size Distribution. *Advances in Nanoparticles*, 4, 37-44.

[21] Yakubu, A., Zulkifly, A., Nor Azowa, I., & Ahmad, F. (2015b). The Effect of ZnO nanoparticles Filler on Complex Permittivity of ZnO-PCL Nanocomposite at Microwave Frequency. *Physical Science International Journal*, *6*(3), 196-202.

[22] Yuqing, Y., You, Y., Hongqing, W., Rui, X., & Guoping, W. (2018). Morphology Control of a Nanoporous Nickel/Cobalt Double Hydroxide for Supercapacitor Electrode Materials using Halides. *International Journal of Electrochemical Science*, 13, 466.